Polarized radiance distribution measurements of skylight: Part 1, system description and characterization.

Kenneth J. Voss and Yi Liu

Physics Department

University of Miami

Coral Gables, Fl. 33124

(305) 284 2323 ext 2, kvoss@umiami.miami.edu

Abstract

A new system to measure the natural sky light polarized radiance distribution has been developed. The system is based on a fisheye lens, CCD camera system, and filter changer. With this system sequences of images can be combined to determine the linear polarization components of the incident light field. In this paper calibration steps to determine the system's polarization characteristics are described. Comparisons of the radiance measurements of this system and a simple pointing radiometer were made in the field and agreed within 10% for measurements at 560 nm and 670 nm and 25% at 860 nm. Polarization tests were done in the lab. The accuracy of the intensity measurements is estimated to be 10%, while the accuracy of measurements of elements of the Mueller are estimated to be 2%.

1. Introduction

The intensity and polarization of skylight have long been studied for many reasons. Early interest involved explaining natural phenomena such as the color of the sky and rainbows.[1,2] Since the discovery of skylight polarization by Arago in 1809, studies on the polarization of skylight and neutral points have been emphasized as these can be used as indicators of atmospheric turbidity.[3,4]

Early measurements of skylight polarization were made mainly by visual means. As the semiconductor technology advanced, new photodetectors in conjunction with computer technology made the automatic measurements of light and its polarization possible. A large number of optical systems have been developed for observations of polarized light in various fields. Coulson[1] lists the various types of polarimeters developed for observations of the earth's atmosphere and surface. Although photomultiplier tubes have been used as detectors for most of the systems, some devices use other detectors such as silicon cells or photographic film for special purposes. Video polarimetry techniques have also been developed using three TV cameras for atmospheric science[5] and CCD cameras for the natural light field.[6] Imaging Stokes polarimetry using CCD image sensors[7] has the advantage of processing data on a pixel-by-pixel basis; thus data over a wide field-of-view can be obtained. The polarimeter described in this paper takes advantage of Stokes polarimetry using a CCD image sensor and a "fisheye" lens as the input optics thus enabling measurement of Stokes parameters over the whole hemisphere.

This system is based on the RADS-II Electro-Optic "Fisheye" Camera Radiance Distribution System.[8] This system uses a "Fisheye" camera lens, a filter changer, and a cooled CCD image sensor to measure a hemisphere of the spectral radiance distribution. With the spectral filter changer, measurement at several spectral bands can be performed in a short time (minutes). By placing dichroic sheet type polarizers in one of the filter wheels, RADS-II becomes an analyzer-type polarimeter (RADS-IIP). With proper calibration, RADS-IIP enables spectral measurement of the skylight polarized radiance distribution. The data process involves taking three data images with the polarizers in different orientations, i.e., the preferred transmission axes oriented in different directions, and these images combined to acquire three of the light field Stokes parameters.

In this paper we will discuss the overall design of the RADS-IIP system, and the calibration steps unique to the polarization system, specifically the characterization of the

instrument in Mueller matrix representation. Radiometric calibration of the RADS system without polarization has been described previously[9] and will not be discussed in detail here; only aspects specific to this system are included and we will show results of a field comparison with a simple unpolarized radiometer. Spectral polarization radiance distribution measurements at different sites, aerosol optical thickness, and sun angles will be presented in a following paper.

2. Background information

It is useful to define the radiometric quantities that we will need. The radiance is defined as the amount of radiant power, d^2P_λ, at wavelength λ, within a wavelength interval $d\lambda$ and a differential solid angle $d\Omega$, which crosses an element of area dA and in the direction making an angle θ to the normal of dA:

$$L_\lambda(\theta,\phi) = \frac{d^2 P_\lambda(\theta,\phi)}{\cos\theta \, dA \, d\Omega \, d\lambda}. \qquad \text{Eq. (1)}$$

Implicit in the radiance is the directional dependence of the quantity. The collection of radiance information for all angles is the radiance distribution. The commonly measured quantities of upwelling and downwelling irradiance (E_u and E_d respectively) are simply defined as the cosine weighted integrals of the radiance distribution over the relevant solid angles.

To describe the polarized radiance distribution we must have a way to represent the polarization of the radiance in a given direction. A convenient representation is provided by the Stokes vector. The electric field vector $\vec{E}$ of the light field can be decomposed into two components, E_l and E_r, which represent the magnitude and phase of the electric field vectors parallel ($\vec{l}$) and perpendicular ($\vec{r}$) to a reference plane:

$$\vec{E} = E_l\vec{l} + E_r\vec{r}. \qquad \text{Eq. (2)}$$

The reference plane is normally defined as the plane containing the incident and scattered beams in scattering problems. Assuming that a coherent electromagnetic wave propagates in the Z direction ($\vec{r} \times \vec{l}$) with a frequency ω, and that amplitudes and phases for the electric fields of an electromagnetic wave in the $\vec{l}$ and $\vec{r}$ directions are a_l, a_r and δ_l, δ_r, respectively, then

$$E_l = a_l \cos(kz - \omega t + \delta_l),\ E_r = a_r \cos(kz - \omega t + \delta_r) \quad \text{Eq. (3)}$$

where $k = 2\pi/\lambda$ is the wave constant. In general, the tip of the electric vector described in Eqs. (2) and (3) forms an ellipse. To describe the elliptically polarized wave three independent parameters, such as those of the Stokes vector,[10] (first introduced by Stokes[11] in 1852) are needed,

$$\begin{aligned} I &= E_l E_l^* + E_r E_r^*, \\ Q &= E_l E_l^* - E_r E_r^*, \\ U &= E_l E_r^* + E_r E_l^*, \\ V &= -i(E_l E_r^* - E_r E_l^*). \end{aligned} \qquad \text{Eq. (4)}$$

For a coherent wave, I, Q, U, and V are real quantities that satisfy the following equation:

$$I^2 = Q^2 + U^2 + V^2 . \qquad \text{Eq. (5)}$$

Assume the ellipse has a major axis (length b) and a minor axis (length c), and the major axis makes an angle χ with the $\vec{l}$ direction. The four Stokes parameters can also be expressed in terms of I, χ, and β ($\tan\beta = c/b$) by direct analyses as:

$$I = I_l + I_r,$$

$$Q = I_l - I_r = I \cos 2\beta \cos 2\chi,$$

$$U = I \cos 2\beta \sin 2\chi,$$

$$V = I \sin 2\beta. \qquad \text{Eq. (6)}$$

In representing the wave using Eqs. (4) or (6), we have assumed a constant amplitude and phase. However, the actual light field consists of many simple waves in very rapid succession. As a result, measurable intensities are associated with the superposition of many millions of simple waves with independent phases. In this case it is straightforward to prove that

$$I^2 \geq Q^2 + U^2 + V^2. \qquad \text{Eq. (7)}$$

The degree of polarization, $P+$, and the degree of linear polarization, *P(linear)*, are useful parameters and can be defined as:

$$P+ = (Q^2 + U^2 + V^2)^{1/2} / I \qquad \text{Eq.(8)}$$

$$P(linear) = (Q^2 + U^2)^{1/2} / I \qquad \text{Eq.(9)}$$

The plane of polarization and the ellipticity are defined as:

$$\tan 2\chi = U / Q, \qquad \text{Eq. (10)}$$

$$\sin 2\beta = V / (Q^2 + U^2 + V^2)^{1/2}. \qquad \text{Eq. (11)}$$

For partially polarized light, the Stokes parameters (I, Q, U, V) can be decomposed into two vectors, a completely unpolarized component and elliptically polarized component as

$$\begin{bmatrix} I \\ Q \\ U \\ V \end{bmatrix} = \begin{bmatrix} (Q^2+U^2+V^2)^{1/2} \\ Q \\ U \\ V \end{bmatrix} + \begin{bmatrix} I-(Q^2+U^2+V^2)^{1/2} \\ 0 \\ 0 \\ 0 \end{bmatrix} \qquad \text{Eq. (12)}$$

Transformation of a Stokes vector, (I_o, Q_o, U_o, V_o), into a new Stokes vector, (I, Q, U, V) by an optical process (scattering, optical elements, reflection, refraction, etc.) can be represented as a linear process with the Mueller matrix:

$$\begin{bmatrix} I \\ Q \\ U \\ V \end{bmatrix} = \begin{bmatrix} M11 & M12 & M13 & M14 \\ M21 & M22 & M23 & M24 \\ M31 & M32 & M33 & M34 \\ M41 & M42 & M43 & M44 \end{bmatrix} \begin{bmatrix} I_o \\ Q_o \\ U_o \\ V_o \end{bmatrix} \qquad \text{Eq. (13)}$$

Consider an optical instrument with elements such as birefringent crystals, sheet polarizers, quarter-wave plates, imaging lenses, filters, etc. In general this instrument may cause absorption, scattering, reflection, and refraction and these actions will be represented by the system's Mueller matrix. If a polarization insensitive detector (such as a CCD array with the light at approximately normal incidence) is placed behind the optical system, then only the intensity (I) of the light exiting the system is measured. In general this intensity is due to the system's Mueller matrix and the Stokes vector of light incident on the system. If the system Mueller matrix is known and variable, it is possible that combinations of measurements may be used to measure the Stokes vector of the incoming light field. For example, when a linear polarizer is used as the optical element, its Mueller matrix can be represented as follows:

$$M_p = \begin{bmatrix} k_1 + k_2 & (k_1 - k_2)\cos 2\psi & (k_1 - k_2)\sin 2\psi & 0 \\ (k_1 - k_2)\cos 2\psi & (k_1 + k_2)\cos^2 2\psi + 2\sqrt{k_1 k_2}\sin^2 2\psi & (k_1 + k_2 - 2\sqrt{k_1 k_2})\cos 2\psi \sin 2\psi & 0 \\ (k_1 - k_2)\sin 2\psi & (k_1 + k_2 - 2\sqrt{k_1 k_2})\cos 2\psi \sin 2\psi & (k_1 + k_2)\sin^2 2\psi + 2\sqrt{k_1 k_2}\cos^2 2\psi & 0 \\ 0 & 0 & 0 & 2\sqrt{k_1 k_2} \end{bmatrix}$$

Eq. (14)

where k_1 and k_2 are the transmittances of the polarizer along the preferred axis and an axis 90° to this axis. ψ is the angle between the polarizer preferred transmittance plane and a reference plane. If a sequence of perfect polarizers (k_1=1 and k_2 = 0) with ψ = 0°, 45°, 90°

are used as analyzers of an incoming Stokes vector (I_o, Q_o, U_o, V_o) then the resulting intensities measured by a detector after the polarizers would be

$$
\begin{aligned}
(\psi = 0°) \qquad & I_1 = I_o + Q_o \\
(\psi = 45°) \qquad & I_2 = I_o + U_o \\
(\psi = 90°) \qquad & I_3 = I_o - Q_o
\end{aligned}
\qquad \text{Eq. (15)}
$$

By combining these measurements three elements of the incoming stokes vector I_o, Q_o and U_o can be determined. If the circular polarization element, V_o, is required than an additional step using a circular polarizer as an analyzer is needed. In general however, light in the atmosphere is not circularly polarized, so we will not measure this quantity. In the ocean, due to the existence of water-air surface, light may undergo total reflection at the surface and return back to the ocean, this process will introduce a small amount of circularly polarized light.[12]

These equations form the basis of analyzer polarimeters, such as the RADS IIP. What must be determined, through the calibration process, are the instrumental Mueller matrix elements with each orientation of the internal polarizers. This calibration process will be discussed below.

3. Instrument description

The development of the electro-optic radiance distribution camera system (RADS) has enabled rapid and accurate measurement of the spectral radiance distribution.[13,8] A block diagram of this system is given in Fig. 1.

The central features of RADS-II are "Fisheye" optics which allows the radiance distribution over a whole hemisphere (of spatial directions) to be imaged on the 2-D image sensor through the imaging optical system, a remotely controlled filter changer assembly which allows the spectral measurement region to be changed rapidly, and, in the case of

RADS IIP, a polarization filter wheel which allows the Mueller matrix of the instrument to be varied. The integration time of the CCD sensor is determined by an electro-mechanical shutter, which is controlled by a computer interface card. Typical image integration times are between 0.5 and 15 seconds; thus measurement takes place rapidly. The acquired image is digitized using a 16 bit A/D converter and the digital images are stored in a hard drive in the associated IBM/PC computer.

The CCD camera system uses a solid state StarScape II CCD camera from First Magnitude Corp.,[14] which adopts the TC215 image sensor from Texas Instrument. The TC215 is a full-frame charged-coupled device (CCD) image sensor that provides high-resolution image acquisition for image-processing applications. The image format measures 12 mm horizontally by 12 mm vertically. The image area contains 1018 active lines with 1000 active pixels per line. Six additional dark reference lines give a total of 1024 lines in the image area, and 24 additional dark reference pixels per line give a total of 1024 pixels per horizontal line. The digitizer adds 32 more dummy lines and 32 more dummy elements each line, thus the actual size of a digital image is 1056 x 1056 pixels. The image acquiring software provides binning features and in all of our images the data were binned into 2x2 pixel samples resulting in a 528 by 528 format; thus the effective pixel size is approximately 24 μm x 24 μm .

A series of lens relay optics transfers the bundle of light rays from the fisheye converter lens, through the spectral and polarization filters, and then forms an image on the CCD array. The final image size is 10.66 mm in diameter for a maximum full angle field of view of 178°, which guarantees the image is well within the 12 mm by 12 mm CCD array. The maximum deviation of light rays from the instrument optical axis, at the position of the spectral interference filters, is 12^0 . This angular dispersion of the light rays is taken into account in the spectral calibration of the instrument system.

A. Dark Noise Analysis

In the CCD sensor, dark noise (signal with no light flux incident) of the whole camera system can be generated by three processes: (a) thermal generation of electrons inside the sensor array, which depends on sensor temperature and is by nature random, (b) readout noise, which depends on readout circuitry, and (c) signal processing noise, which depends on the signal processing (A/D converter) circuitry. In normal operation the thermo-electrically cooled TC215 image sensor temperature ranges from -30° to -40° to reduce the thermal generation of electrons.

Dark images were obtained by keeping the shutter closed while the CCD was integrating. Fig. 2 is the typical dark count pattern along a row and column of the same image. Inactive and dummy pixels on the edges of the image manifest themselves in both graphs on the left and right sides. As shown, the dark current in an image is far from uniform. Figure 3 is the variation in the average dark current of a central area of 10 by 10 pixels on the image as a function of time and sensor temperature. This shows that the dark current increases linearly as we increase the integration time and increases exponentially as the sensor temperature increases, as expected.[15] In all experiments, dark images were measured immediately after data images, keeping the same integration time and temperature. These dark images are subtracted from the data images during data processing.

Careful investigation of a series of dark images shows that there is also random noise after the subtraction. In order to reduce this random noise, a series of dark images were taken under the same conditions. Images were then added, and the standard deviation of the whole image was calculated as each image was added. Application of a 3 x 3 averaging filter to the subtracted image is sufficient to maximize the reduction of this random noise.

B. Crosstalk Effect

Pixel crosstalk can be defined as the interaction between the individual detector elements of an array detector. Blooming is a particular form of spatial crosstalk that affects most array detectors. This phenomenon arises when a pixel or a localized group of pixels is over exposed to light. Blooming has appeared while using TC215 imager and manifests itself as spilling of charge from saturated pixels into neighboring unsaturated pixels on the same column. Thus the information content of neighboring pixels is destroyed. This effect can limit the accuracy and dynamic range of the sensor and is avoided by adjusting the neutral density filter or exposure time to prevent saturation. In the sky radiance distribution measurements, an occulter has been adopted to block the direct solar radiation in all field experiments to avoid this effect and to avoid camera lens "flaring".

The row-column crosstalk phenomenon[16] was also found on the TC215 image sensor. The existence of this effect requires a correction algorithm be applied in image processing programs in order to offset this interaction between pixels. Row-column crosstalk means that the signal in a single pixel will affect another pixel on the same row. Investigations were made to gain qualitative and quantitative characterization of the phenomenon. An experiment was performed which illuminated only the central portion of the array. A typical result is shown in Fig. 4. In this figure, there are two lines; one line is the signal from the pixels of the selected row after the pixels in the illuminated region were exposed to light (peak between 300 and 400), the other line is the same row in a corresponding dark image. While counts in the illuminated pixels increased substantially, the counts from pixels in the nonilluminated region decreased significantly with respect to dark counts. This decrease is due to row-column crosstalk effect and is proportional to the counts in the illuminated region. A row-column crosstalk correction can be accomplished by determining the crosstalk signal for all pixels located on a given row and subtracting this from the net signal of each pixel on that same row. The crosstalk signals for all rows in an image are determined by the signals in a single column in the dark area of the data image;

this single column then is duplicated to form a crosstalk signal image in which every column has the exact same information. The correction for the entire data image can be achieved by subtracting this crosstalk signal image from the data image.

C. Shutter control

An experiment was performed to test the shutter-controlling signals and the accuracy of the exposure timing. The period of the signal opening the shutter was measured for a series of specified integration times. The result was that all input times agree with measured times within 0.2% in a range of 100ms to 50s. Due to the reaction time of the shutter and the finite opening and closing times, a maximum 5 ms absolute error may still exist; thus in the field we use integration times longer than 0.5 seconds, which makes the maximum error from this source approximately 1%.

4. Calibration

The objective of the RADS-IIP calibration is to obtain a functional relationship between the incident flux and polarization, and the instrument output. The calibration of the instrument requires a functional set of data concerning the spectral, spatial, and polarization characteristics of the instrument.[17] Voss and Zibordi[9] discussed the steps required for radiometric scalar (non-polarized) calibration of a fisheye camera system. Calibration of the system linearity, spectral response, camera system rolloff, and absolute system response were performed by these methods. Only the results of these steps will be discussed.

A. Linearity and Spectral Calibration

Figure 5 shows the result of a test of the system linearity. In the experimental setup a barium sulfate reflectance plaque was illuminated in the normal direction by a stable 1000W lamp providing source of stable radiance for the camera. The camera viewed the plaque at a direction 45 degrees to the normal. The light intensity incident on the array was controlled

by changing the integration time, and an average of 3 by 3 pixels in the center of the image was obtained. This result shows that the camera output is not exactly linear but can be defined accurately over three orders of magnitude by a simple power function, with an exponent of 1.04.

Interference filters are used in the RADS system to select the spectral band of interest. A calibration was performed to determine the spectral response of the camera system by illuminating the system with light from a monochrometer and measuring the system response. Spectral filters 1-4 were found to be centered at 439 nm, 560 nm, 667 nm, and 860 nm, with full width at half maximum of 10.5 nm, 10.0 nm, 11.0 nm, and 13.5 nm respectively.

Figure 6 is a typical system rolloff curve determined in the calibration process; the method is described in Voss and Zibordi.[9] This curve was found to be rotationally symmetric around the optic axis of the camera system, so the regression curve shown was used in the data reduction process. An absolute calibration of the system response was also done using a 1000 W lamp (FEL standard lamp traceable to NIST) and a Spectralon reflectance plaque.

B. Polarimatric Calibration

The Mueller matrix of the camera optical system can be represented as a single 4 x 4 matrix. Although in theory this Mueller matrix of the optical system can be decomposed into a chain of matrices that are representations of the individual optical components, it is better to calibrate the system as one unit using prepared sources of partially polarized light. Since the CCD array only measures intensity, only the first row of the total system Mueller matrix must be determined. In this case we input known sets of I_o, Q_o, U_o, and V_o, I is measured,

and *M11*, *M12*, *M13*, and *M14* can be determined. A convenient set of Stokes vectors to use as input beams are:[18]

$$A=\begin{bmatrix} I_o \\ I_o \\ 0 \\ 0 \end{bmatrix}, B=\begin{bmatrix} I_o \\ -I_o \\ 0 \\ 0 \end{bmatrix}, C=\begin{bmatrix} I_o \\ 0 \\ I_o \\ 0 \end{bmatrix}, \text{and } D=\begin{bmatrix} I_o \\ 0 \\ 0 \\ I_o \end{bmatrix}. \qquad \text{Eq. (16)}$$

where A is horizontally polarized light, B is vertically polarized light, C is +45° polarized light, and D is right-handed circularly polarized light. These beams are sequentially input into the optical system and the output light intensity recorded in each case. This provides four linear equations, the solution of which determines the required elements of the system Mueller matrix.

Since we produce the linear polarization states with a dichroic sheet polarizer (Gray polarizing film, Edmund Scientific)[19] we need to measure the spectral polarization and transmission properties of this polarizer. The principal transmittances of the dichroic polarizers used were measured and are shown as functions of wavelength in Fig. 7. The extinction ratios, i.e., the fraction of light transmitted through a closed pair of polarizers, were found to be less than 1% for visible light. Transmission for a single dichroic polarizer acting alone, ranges from 5% to 50% for visible light. Thus using sheet polarizers and an unpolarized light source, one can generate the following light beams as input light:

$$A=\begin{bmatrix} 1 \\ \dfrac{k_1-k_2}{k_1+k_2} \\ 0 \\ 0 \end{bmatrix}, B=\begin{bmatrix} 1 \\ \dfrac{-k_1+k_2}{k_1+k_2} \\ 0 \\ 0 \end{bmatrix}, C=\begin{bmatrix} 1 \\ 0 \\ \dfrac{k_1-k_2}{k_1+k_2} \\ 0 \end{bmatrix}. \qquad \text{Eq. (17)}$$

In general the ingoing light undergoes interactions with various optical components of the RADS. If we number each individual optical element in the order of their presence,

then the Mueller matrix can be described by the Mueller matrix of a chain of total number of optical components as follows:

$$M = ...M_3\, M_2\, M_1\,, \qquad \text{Eq. (18)}$$

where M_i is the Mueller matrix of the i-th optical component. For our RADS-II system, these optical components are lenses, polarizers, interference color filters, and absorption neutral density filters. For the convenience of our analysis, let us denote the Mueller matrix of the polarizer as M_p. Light interacting with the surfaces of optical components undergoes refraction for lenses, reflection and refraction for interference filters, absorption and refraction for neutral density filters.

The Mueller matrix for an isotropic absorption process is the unity matrix (note that below all Mueller matrices are normalized to M11, and therefore we use the term of reduced Mueller matrix). The reduced Mueller matrix for reflection and refraction processes has been derived by Kattawar and Adams[20] and has the following form:

$$\begin{bmatrix} 1 & \frac{\alpha-\eta}{\alpha+\eta} & 0 & 0 \\ \frac{\alpha-\eta}{\alpha+\eta} & 1 & 0 & 0 \\ 0 & 0 & \frac{\gamma}{\alpha+\eta} & 0 \\ 0 & 0 & 0 & \frac{\gamma}{\alpha+\eta} \end{bmatrix} \qquad \text{Eq. (19)}$$

where α, η, and γ depend on incident and refracted angles. These matrix elements are plotted in Fig. 8 as a function of incident angle assuming light entering glass (relative index of refraction, 1.5).

The product of a chain of matrices with the form of Eq. (19) has the same symmetry as Eq. (19), and this allows us to write the total Mueller matrix as the product of the polarizer Mueller matrix and the Mueller matrix for all other optical components. In doing so we have made an assumption that all the contributions to the camera's Mueller matrix due to

optical components other than polarizers are from optical components before the polarizer, mainly due to the fish-eye input optics. This is reasonable because only at the input stage are large refraction angles involved. Even for the interference filter, every transmitted ray undergoes two refractions and pairs of reflections. The reduced Mueller matrix for double reflections at small angles is close to unity and therefore the reduced Mueller matrix for an interference filter is nothing but double refraction at small angles, which is also close to a unity matrix. The validity of these assumptions will be tested by experiment. Let M_s be the Mueller matrix due to optical components other than the polarizer; then we can write the total Mueller matrix as:

$$M = M_p M_s \qquad \text{Eq. (20)}$$

Once k_1 and k_2 for polarizers are known, the Mueller matrix, M_p, can be calculated. Thus it is only necessary to measure the Mueller matrix for the camera without a polarizer and the orientation of the polarizer.

In the following discussions, we use the notation m12(W1), m13(W1) and m14(W1) to denote the reduced Mueller matrix elements for the polarization filter wheel in position 1 and m12(W2), m13(W2) and m14(W2) for reduced Mueller matrix elements for the second position. Similar notations will be used to describe the Mueller matrix elements for the third and fourth polarizer positions. There is no polarizer in position 1, but the polarizers in positions 2, 3, and 4 are oriented at 0°, 45°, 90° relative to an arbitrary axis.

Figure 9 shows that the measured m14 values for the four filter wheel locations are close to zero as expected from the form of Eq. (19). The deviations from zero are caused by the imperfect quarter-wave plate employed in the experiment. As we used a quarter-wave plate (at 550nm, Melles Griot 02WRM009) made of mica, it can only approximate a quarter-wave plate at the wavelengths of the RADS-II. The Mueller matrix elements m12 and m13 are shown in Figs. 10 and 11. It can be seen that m13(W1) and m14(W1) are

close to zero. These are the Mueller matrix elements of the camera without a polarizer. But m12(W1) is not zero and varies with incidence angle as T12/T11 of Fig. 8. These results show that the total Mueller matrix of the camera (without polarizers) is similar to Eq. (19).

Experimentally m12(W1) and m13(W1) were found to be rotationally symmetric around the optical axis. Similar experiments were also performed to test for spectral dependence, and it was found that the Mueller matrix is independent of wavelength within experimental error. In each of these cases the system was found to be rotationally symmetric, and spectrally constant within 1%.

With this method we have the following reduced Mueller matrix elements: m12(W1), m13(W1) = m14(W1) = 0. Applying symmetry principles to the Mueller matrix and considering there are only reflections and refractions involved in the camera case (without polarizer), the overall Mueller matrix has the same form as Eq. (19). Thus we can assume m33(W1) = m44(W1) = 1, m23(W1) = m24(W1) = m34(W1) = 0, and the Mueller matrix for the camera (in Eq. (20)) is known. Since the Mueller matrix for a sheet polarizer is known, we are able to generate the Mueller matrix of the RADS-II for any direction of view once the preferred transmission axis of the polarizer is known.

5. Calibration tests

To confirm the accuracy of the scalar (non-polarized) calibration procedures, an experiment was performed in April 1994 in Key West, Florida in conjunction with the Hand Held Contrast Reduction Meter (HHCRM).[21] Measurements of the sky radiance distribution using RADS-II (without polarizers in place) were obtained at 3 wavelengths common to both instruments, 558, 673, and 866 nm. The measurement site was located at the edge of Key West, Florida.

While the RADS-II measurement was obtained quickly (typical integration time was 1 second), the HHCRM measurement had to be taken successively one point at a time. Only

principal plane and almucantor data were taken using the HHCRM. The almucantor corresponds to directions with the same sun-zenith angle but varying azimuthal angles from the sun. The principal plane is composed of directions in the plane containing the sun and the zenith. The HHCRM measurement sequence took about three minutes for each wavelength. In the RADS-II measurements an occulter was used to block the direct solar radiation due to the dynamic range limitation of CCD sensor and to prevent flare from the direct solar beam in the camera optics. Thus no data is available within 20 degrees of the sun in the radiance image.

Figures 12 and 13 compare the RADS-II data with the HHCRM data for three channels at wavelengths of 560 nm, 667 nm and 860 nm. It should be noted that the HHCRM has an approximate pointing inaccuracy of 2 degrees. Figure 14 shows the relative difference of the data in the principal plane for three channels. The difference is computed as:

$$\% \text{ difference} = 100 \times \frac{HHCRM - RADS}{(HHCRM + RADS)/2} \qquad \text{Eq. (21)}$$

The Principal plane is a more difficult comparison because of pointing inaccuracies in the HHCRM and because the rolloff calibration in the RADS system enters strongly into the RADS data set.

For 560 and 670 nm all the data shown have less than a 10 percent difference. The agreement between RADS-II data and HHCRM data for 860 nm is poor, the difference can reach as big as 25% when the radiance value is small, with RADS-II data always higher. The gain of the HHCRM is very sensitive to temperature at this wavelength; thus, the HHCRM data may not be as accurate at this wavelength.

To test the polarization calibration method (separation of polarizer and camera Mueller matrices) an experiment was performed to measure the Mueller matrix elements directly and compare with those same elements obtained by matrix transformation (Eq. (20)). The experimental setup is similar to the absolute calibration method in the way the camera was

placed and light source arranged. An additional device prepared light beams A, B and C as in Eq. (17) and the camera viewed a reflectance plaque, illuminated by a 1000W lamp, through this device. This device is basically a hollow cylinder painted black with a sheet polarizer placed on a polarizer holder in front of the cylinder. The polarizer can be rotated around the cylinder's axis precisely. The aperture of the polarizer allowed a 4 degree field of view. While tests were done for all three wavelengths, Fig. 15 and 16 show the comparisons between experimental results and matrix transformation results for 560 nm. The transformed values differ from the directly measured values only by 1 to 2 %. The development of the matrix transformation technique for RADS-II polarimetric calibration allows the Mueller matrix elements to be computed relatively quickly for the whole hemisphere.

VI) Camera System Mueller Matrix Elements for the Whole Hemisphere

So far we have illustrated the polarimetric calibration procedures for the RADS-II CCD camera system. Since the Mueller matrix elements depend on the coordinate system, it is necessary to define the coordinate system used.

Consider an x-y coordinate system on the CCD array with z pointing normal to the array. All the Mueller matrix elements are represented in this x-y-z coordinate system for the RADS-II optical system and in describing the radiative transfer process. For the optical system of RADS-IIP, each pixel on the array corresponds to a zenith and azimuth angle. The *l* axis of the system is in the plane defined by the specific look direction and the optic axis of the system. The zenith and azimuth angles determine the Mueller matrix elements and therefore determine the polarization signature of the camera system. In the previous discussions, we have shown that Mueller matrix of the camera does not depend on azimuth angle (rotationally symmetric around the optic axis). Since we know the geometric mapping of spatial direction to individual pixel on the array, it is possible to express the spatial Mueller matrix in an image format.

The following figures (Figs. 17 - 18) are example contour plots of the Mueller matrix element images for M12 and different configurations of polarizers, all generated by using Eq. (20). The rotational symmetry is evident in those images. M12(W1) only slowly varies with off-axis zenith angle. M12(W2) varies strongly with zenith angle as the incoming *l* axis is oriented parallel and perpendicular to the transmission axis of the polarizers orientation, shown in Fig. 17. M12(W3) (shown in Fig. 18) and M12(W4) are similar only rotated at 45° azimuthally to follow the rotation of the polarizer. With these (effectively) images of the Mueller matrix elements, the Mueller matrix of the camera system is defined exactly. These images then provide a convenient way to store this information and operate on data acquired in the field.

7) Conclusion

We have described the RADS-IIP instrument and have shown through experiment that the system performs well. We expect that the absolute calibration of the system is accurate with 10% for most channels. Polarization measurements are accurate within approximately 2%. With the images resulting from the polarimetric calibration we can process sets of sky radiance distribution data to obtain polarized spectral radiance distributions accurately and quickly (<2 min.) for all directions. Because all directions are taken simultaneously the system is well adapted to operate in a changing environment or on a less stable platform, such as a ship. In a companion paper we will present data obtained with the instrument and investigate aspects of the sky light polarization.

8) Acknowledgments

The authors would like to acknowledge the support of the Ocean Optics Program at ONR, under grant N000149510309 and NASA under NAS5-31363. Also we would like to thank Albert Chapin for his help during the calibrations.

References

1) K. L. Coulson, *Polarization and intensity of light in the atmosphere*, A. Deepak publishing, Hampton Va. USA (1988).

2) A. T. Young, "Rayleigh Scattering", Physics Today, Jan 1982, 42-48.

3) K. L. Coulson, "Characteristics of skylight at the zenith during twilight as indicators of atmospheric turbidity, I: Degree of Polarization", Appl. Opt., 19, 3469 - 3480 (1980).

4) H. H. Kimball, "The effect of the atmospheric turbidity of 1912 on solar radiation intensities and skylight polarization," Bul. Mt. Weather Observatory, 5, 295 - 312 (1913).

5) T. Prosch, D. Hennongs, and E. Raschke, "Video polarimetry: a new imaging technique in atmospheric science", Appl. Opt., 22, 1360 - 1363 (1983).

6) T. W. Cronin, N. Shashar, and L. Wolff, "Portable imaging polarimeters" in IEEE Proc of the 12th IAPR International conference on pattern recognition, (IEEE Computer Society, Los Alamitos, Ca., 1994), pp. 606- 609

7 H. Povel, "Imaging stokes polarimetry with modulators and charge coupled-device image sensors", Optical Engineering, 34, 1870 - 1878 (1995).

8) K. J. Voss and A. L. Chapin, "Next generation in-water radiance distribution camera system", SPIE Vol. 1750, Ocean optics XI, 384 -387 (1992).

9) K. J. Voss and G. Zibordi, "Radiometric and geometric calibration of a visible spectral electro-optic 'fish-eye' camera radiance distribution system, J. Atmos. Ocean. Tech., 6, 652 -662 (1989).

10) H. C. Van de Hulst, *Light Scattering by Small Particles*, Dover Publications, Inc. (1981).

11) G. G. Stokes, "On the composition and resolution of streams of polarized light from different sources", Trans. Cambridge Phil. Soc., 9, 399 (1852).

12) G. W. Kattawar and X. Xu, "Detecting Raman scattering in the ocean by use of polarimetry", SPIE Vol. 2258, Ocean Optics XII, 222 - 233 (1994).

13) K. J. Voss, "Electro- optic camera system for measurement of the underwater radiance distribution," Opt. Engineering, 28, 241 -247 (1989).

14) P. J. Johnson, "Manual on Starscape II CCD cameras", First Magnitude Inc., Laramie, Wy. (1992).

15) J. S. Campbell, "TC271 Characterization Report", Area array image sensor products, Data book, Texas Instruments, Dallas, Tx.(1994).

16) G. R. Sims and M. B Denton, "Spatial pixel crosstalk in a charge-injection device", Opt. Eng., 26, 999 - 1007 (1987).

17) C. L. Wyatt, *Radiometric calibration: Theory and Methods*, Academic Press, New York (1978).

18) B. J. Howell, "Measurement of the polarization effects of an instrument using partially polarized light", Appl. Opt., 18, 809 -812 (1979).

19) E. H. Land, "Some aspects of the development of sheet polarizers", J. Opt. Soc. Am., 41, 957 - 963 (1951).

20) G. W. Kattawar and C. N. Adams, "Stokes vector calculations of the submarine light field in an atmosphere-ocean with scattering according to a Rayleigh phase matrix: effect of interface refractive index on radiance and polarization", Limnol. Oceanogr., 34, 1453-1472 (1989).

21) W. H. Wilson, "Measurements of atmospheric transmittance in a maritime environment", in Proceedings of the Society of Photo-Optical Instrumentation Engineering, Atmospheric Effects on Radiative Transfer, Vol 195, Sand Diego, 29-30 August, 1979.

Figures

Fig. 1) Block diagram of RADS-IIP instrument.

Fig 2) Dark counts (row) and (column). Illustrates the non-uniformity of the dark signal on the detector. Integration time was 1 s, sensor temperature was -34.5 °C.

Fig 3) Dark counts as a function of integration time and sensor temperature. Illustrates linear relation of dark counts with integration time and exponential relation with sensor temperature.

Fig 4) Cross talk experiment which illustrates the suppression of counts from pixels in the same row as a bright pixel.

Fig 5) Linearity calibration. Line is a power fit to the data and fits well over three order of magnitude of light intensity (exponent is 1.04).

Fig 6) Typical rolloff curve found through calibration process.

Fig 7) Measured principal transmittances for the dichroic polarizer used as a function of wavelength.

Fig 8) Non-zero matrix elements for the reflected and transmitted light due to interaction with a glass (index of refraction = 1.5) surface.

Fig 9) Reduced matrix element M14 as a function of off-axis angle and polarization filter position.

Fig 10) Reduced matrix element M12 as a function of off-axis angle and polarization filter position.

Fig 11) Reduced matrix element M13 as a function of off-axis angle and polarization filter position.

Fig 12) Almucantor comparison of HHCRM and RADS.

Fig 13) Principal plane comparison of HHCRM and RADS.

Fig 14) Relative difference between HHCRM and RADS measurements in the principal plane at each wavelength.

Fig 15) M12 direct measurement and matrix transformation method, illustrating how well the matrix transformation method works to estimate the system Mueller matrix.. Measurements performed at 560 nm.

Fig 16) M13 direct measurement and matrix transformation method, illustrating how well the matrix transformation method works to estimate the system Mueller matrix. Measurements performed at 560 nm.

Fig 17) M12(W2)

Fig 18) M12(W3)

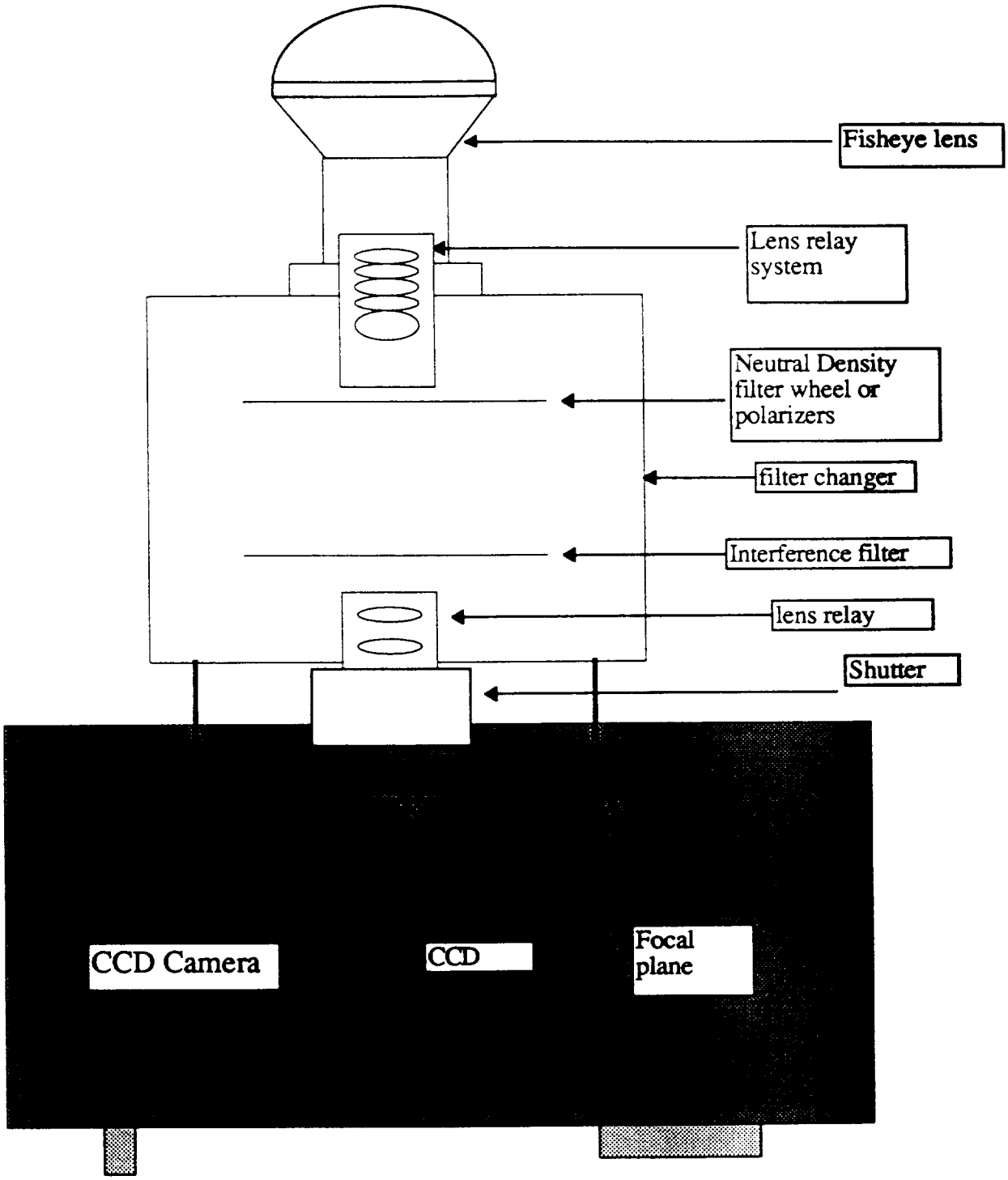
Fisheye lens
Lens relay system
Neutral Density filter wheel or polarizers
filter changer
Interference filter
lens relay
Shutter
CCD Camera
CCD
Focal plane

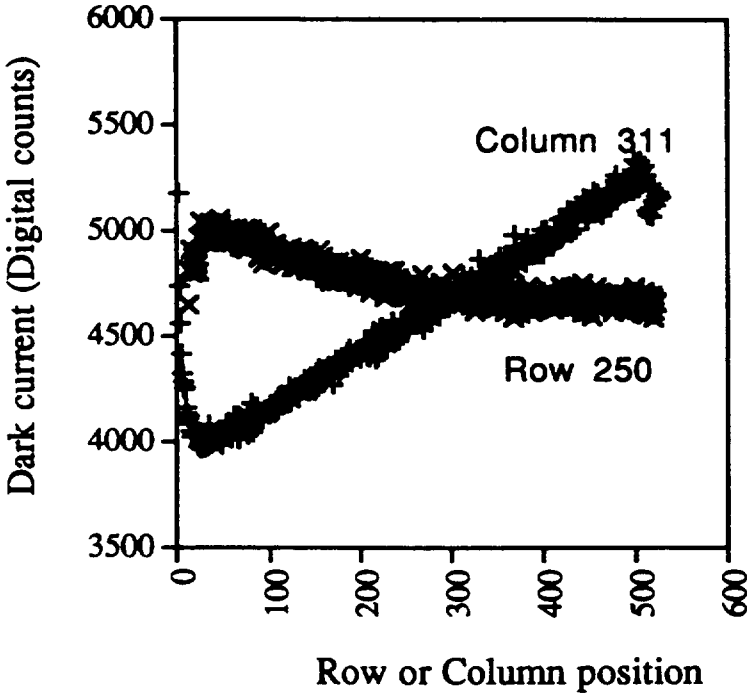
6000
5500
5000
4500
4000
3500
Dark current (Digital counts)
Column 311
Row 250
0
100
200
300
400
500
600
Row or Column position

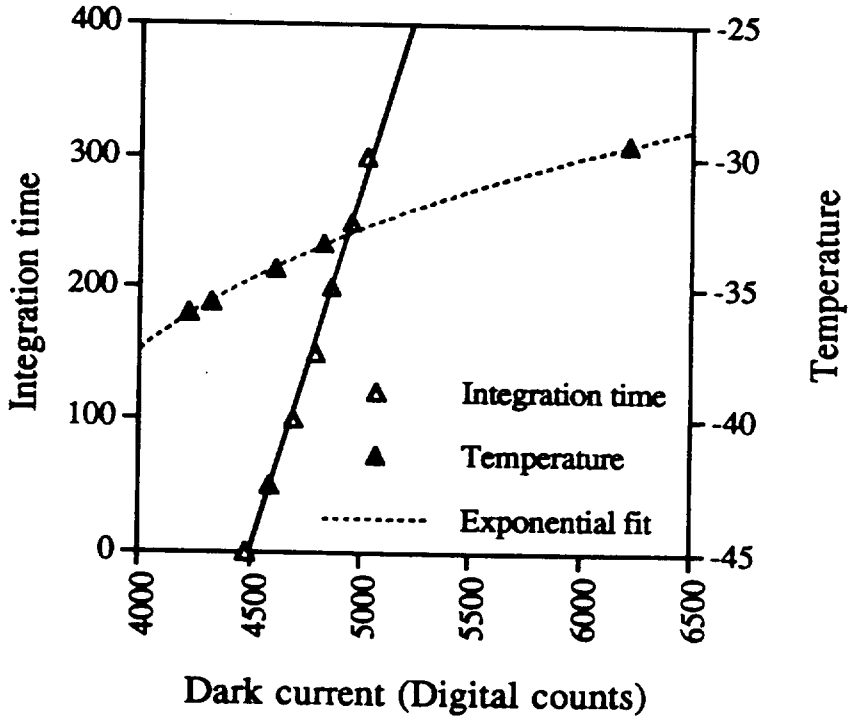
400
300
200
100
0
Integration time
-25
-30
-35
-40
-45
Temperature
Integration time
Temperature
Exponential fit
4000
4500
5000
5500
6000
6500
Dark current (Digital counts)

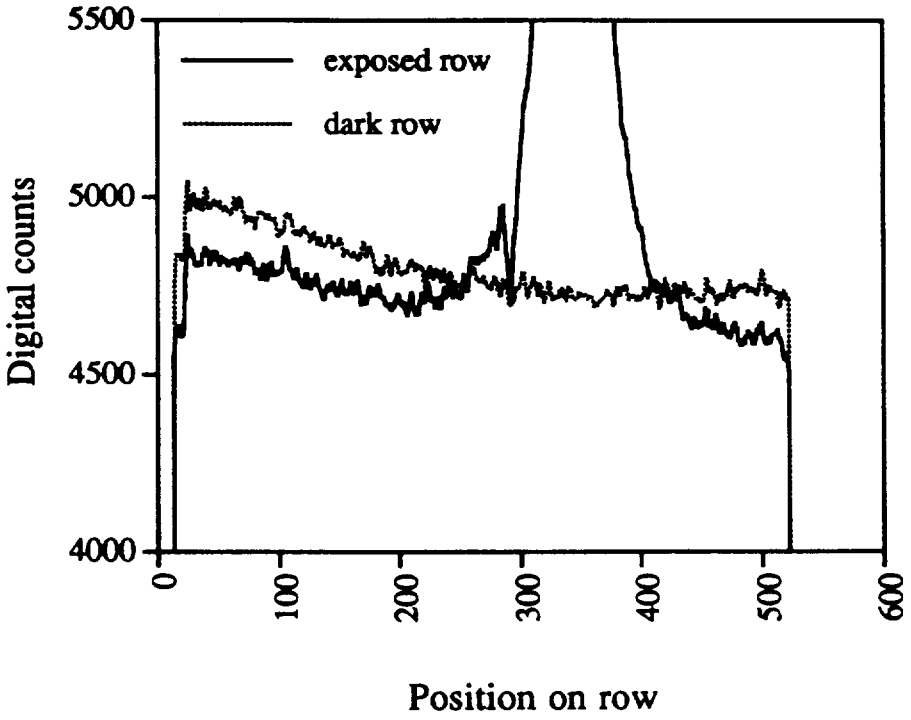
5500
5000
4500
4000
exposed row
dark row
Digital counts
0
100
200
300
400
500
600
Position on row

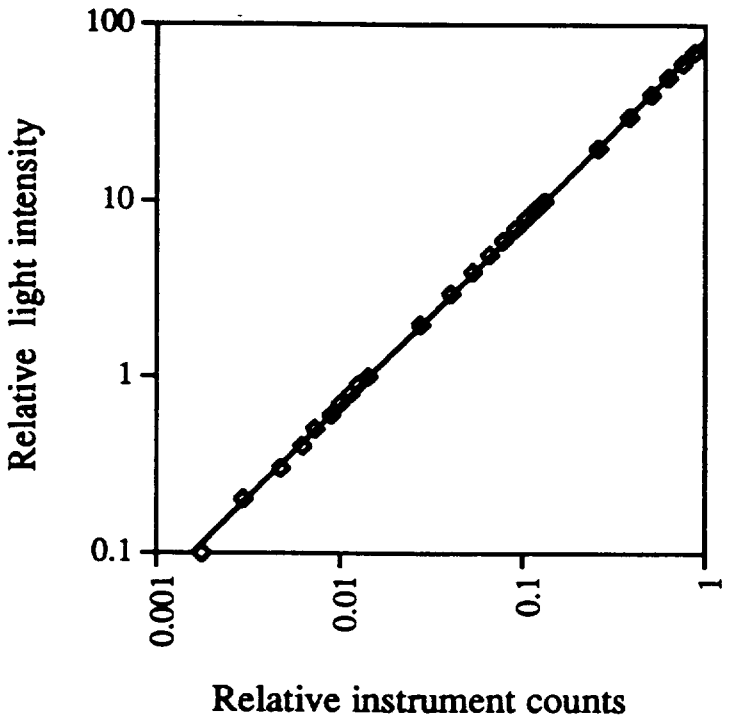
100
10
1
0.1
Relative light intensity
0.001
0.01
0.1
1
Relative instrument counts

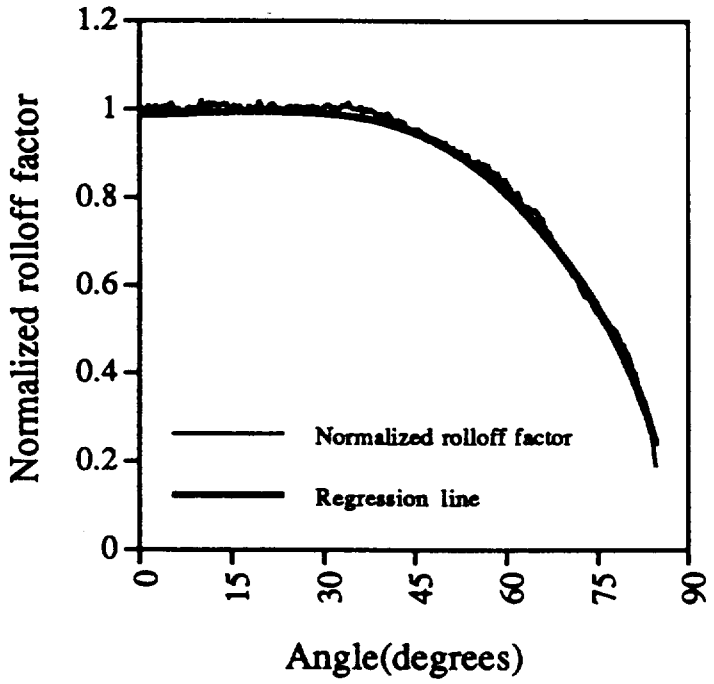
1.2
1
0.8
0.6
0.4
0.2
0
Normalized rolloff factor
Normalized rolloff factor
Regression line
0
15
30
45
60
75
90
Angle(degrees)

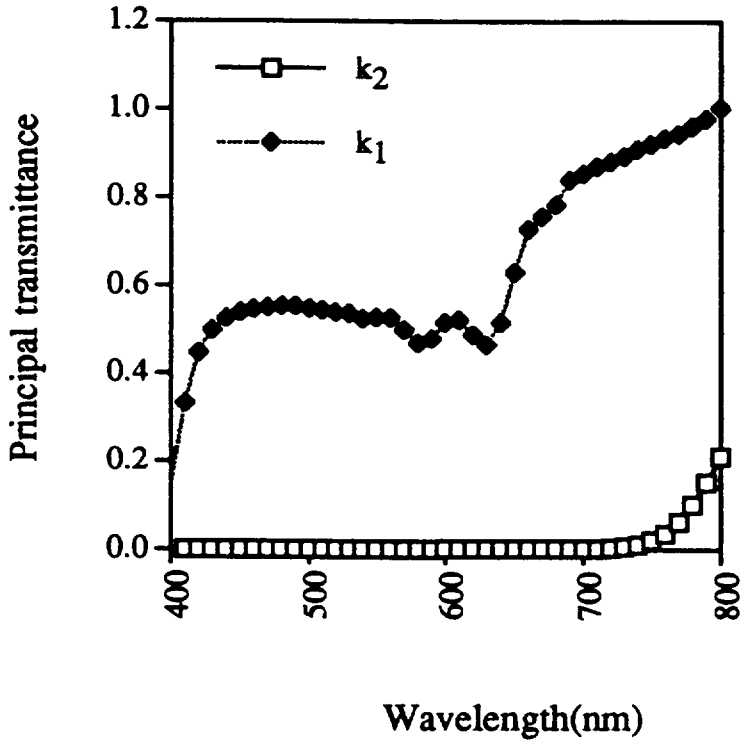
1.2
1.0
0.8
0.6
0.4
0.2
0.0
Principal transmittance
k2
k1
400
500
600
700
800
Wavelength(nm)

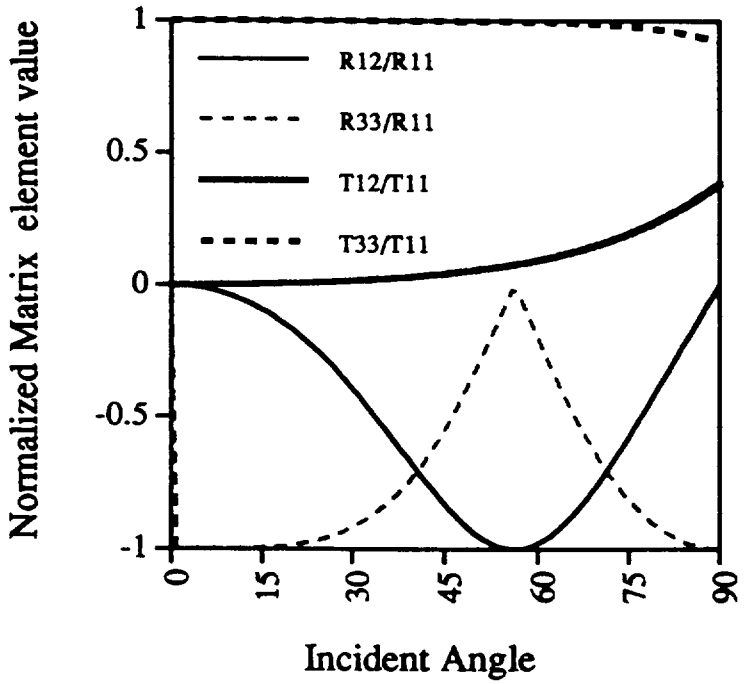
Normalized Matrix element value
1
0.5
0
-0.5
-1
R12/R11
R33/R11
T12/T11
T33/T11
0
15
30
45
60
75
90
Incident Angle

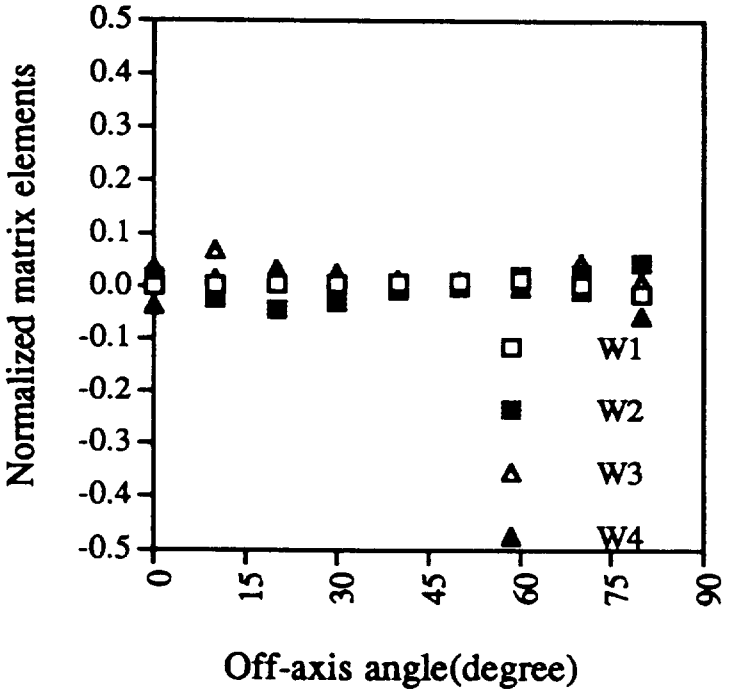
0.5
0.4
0.3
0.2
0.1
0.0
-0.1
-0.2
-0.3
-0.4
-0.5
Normalized matrix elements
0
15
30
45
60
75
90
Off-axis angle(degree)
W1
W2
W3
W4

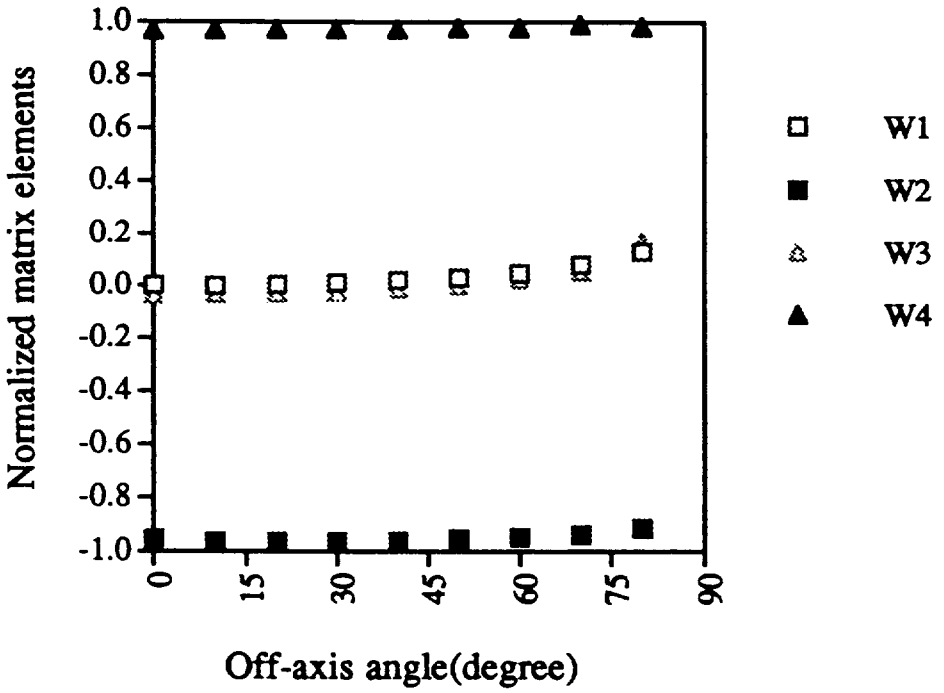
Normalized matrix elements
1.0
0.8
0.6
0.4
0.2
0.0
-0.2
-0.4
-0.6
-0.8
-1.0
0
15
30
45
60
75
90
Off-axis angle(degree)
W1
W2
W3
W4

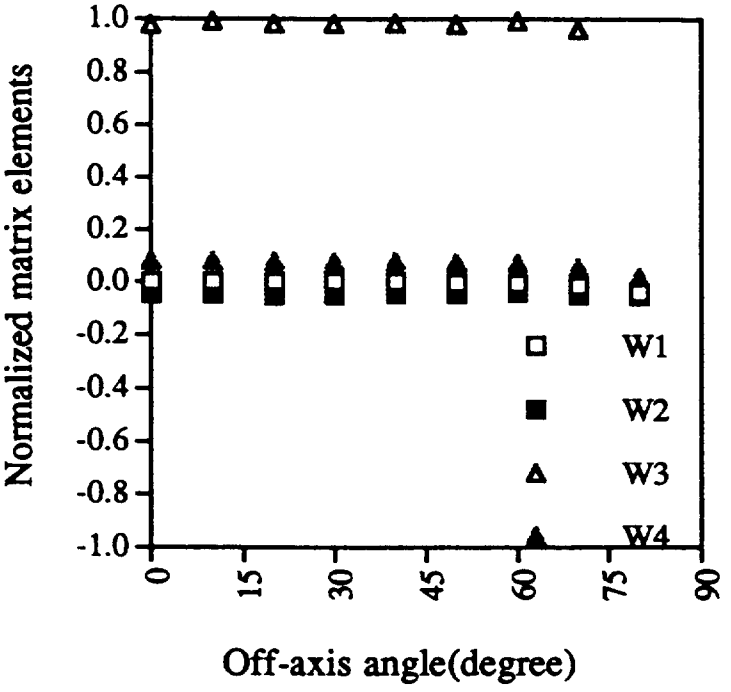
Normalized matrix elements
1.0
0.8
0.6
0.4
0.2
0.0
-0.2
-0.4
-0.6
-0.8
-1.0
0
15
30
45
60
75
90
W1
W2
W3
W4
Off-axis angle(degree)

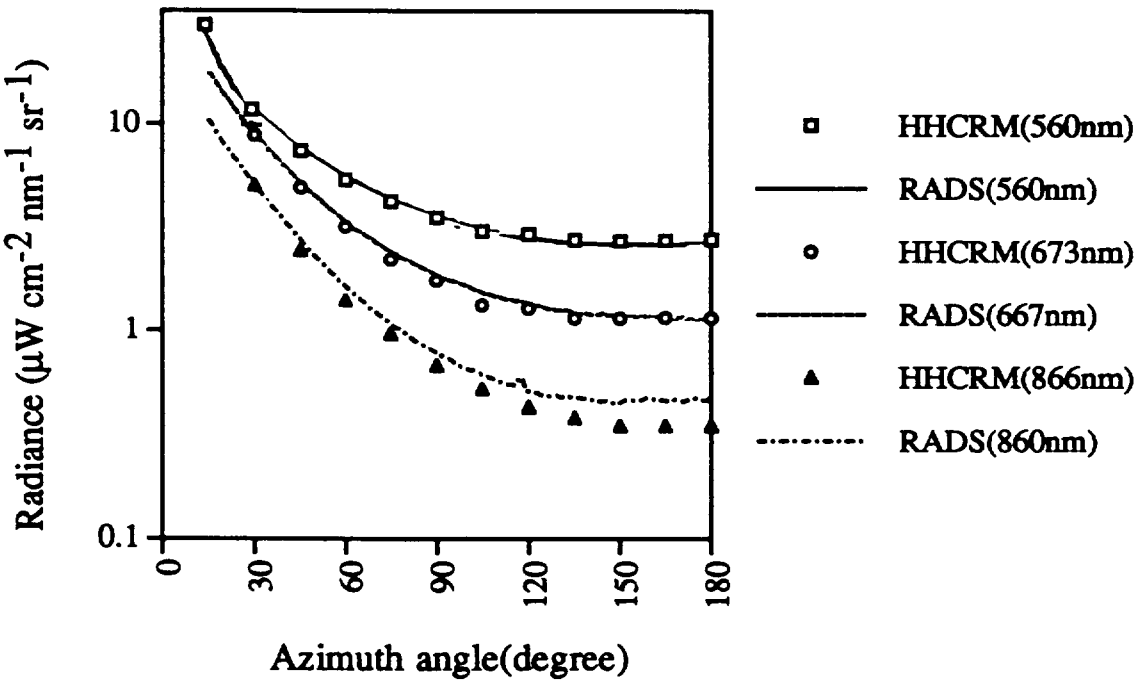
Radiance (μW cm-2 nm-1 sr-1)
10
1
0.1
0
30
60
90
120
150
180
Azimuth angle(degree)
HHCRM(560nm)
RADS(560nm)
HHCRM(673nm)
RADS(667nm)
HHCRM(866nm)
RADS(860nm)

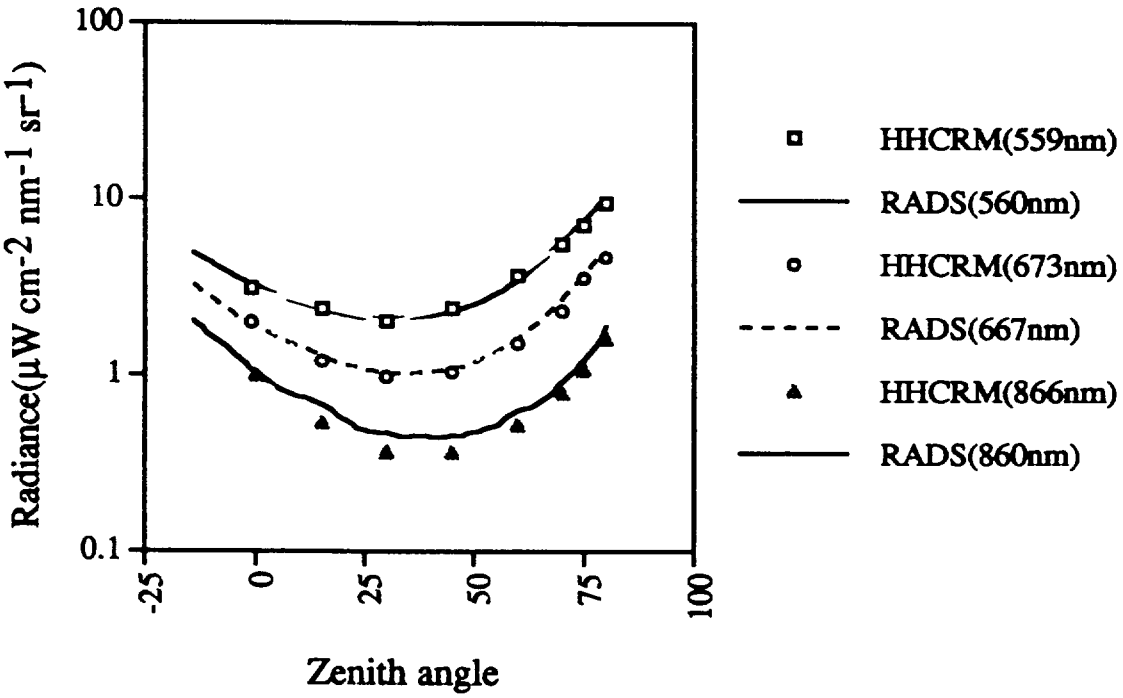
100
10
1
0.1
Radiance(μW cm-2 nm-1 sr-1)
-25
0
25
50
75
100
Zenith angle
HHCRM(559nm)
RADS(560nm)
HHCRM(673nm)
RADS(667nm)
HHCRM(866nm)
RADS(860nm)

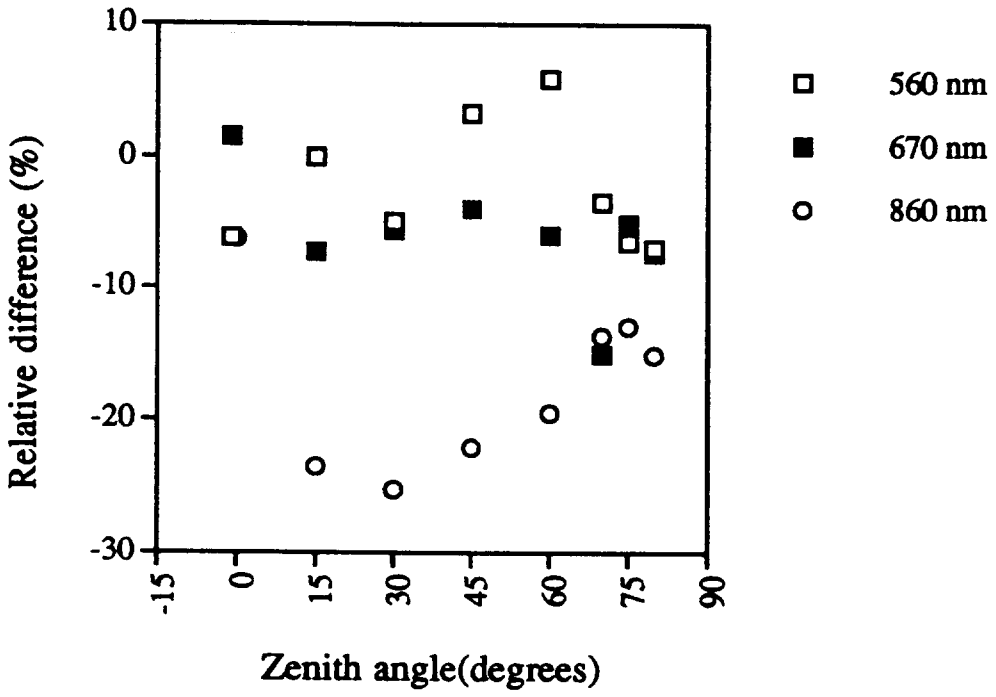
10
0
-10
-20
-30
Relative difference (%)
-15
0
15
30
45
60
75
90
Zenith angle(degrees)
560 nm
670 nm
860 nm

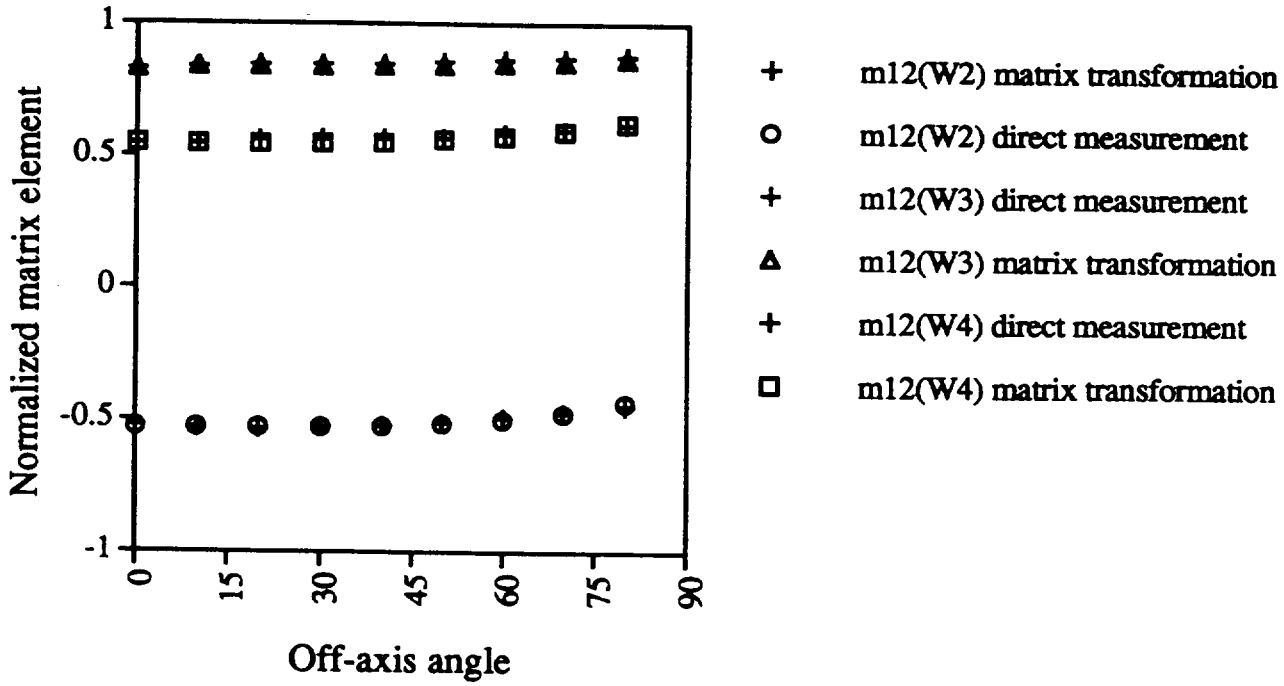
1
0.5
0
-0.5
-1
Normalized matrix element
0
15
30
45
60
75
90
Off-axis angle
m12(W2) matrix transformation
m12(W2) direct measurement
m12(W3) direct measurement
m12(W3) matrix transformation
m12(W4) direct measurement
m12(W4) matrix transformation

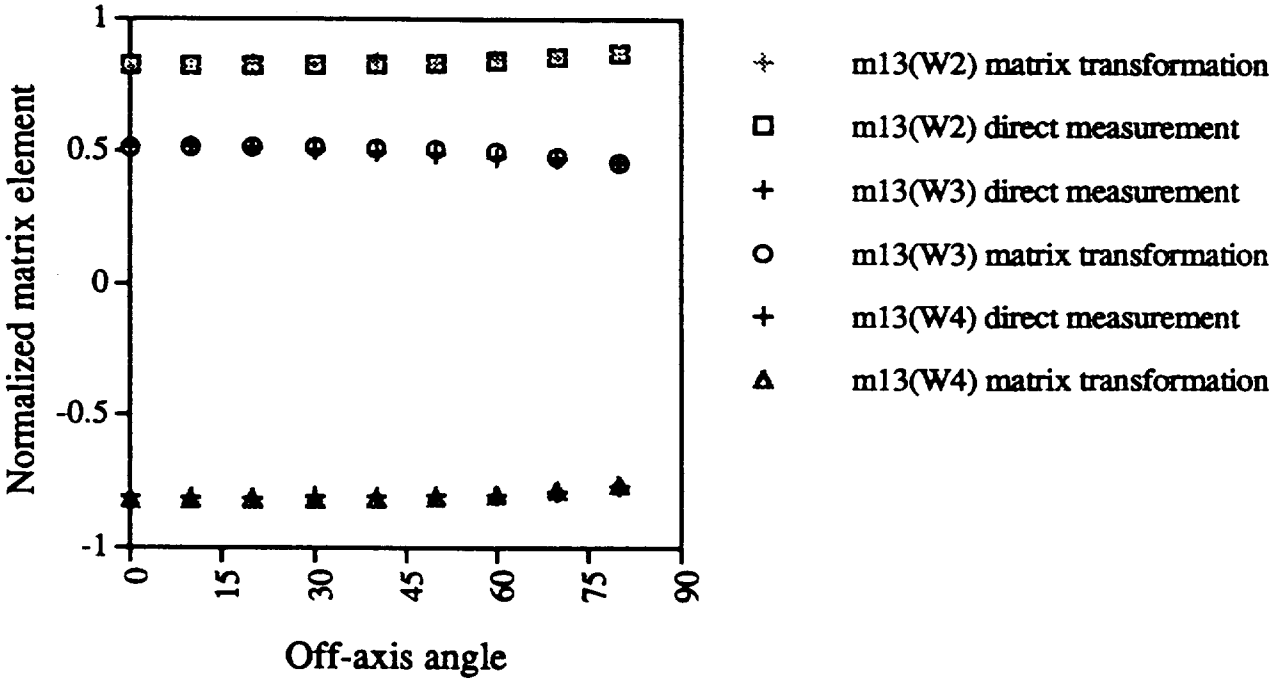
Normalized matrix element
1
0.5
0
-0.5
-1
0
15
30
45
60
75
90
Off-axis angle
m13(W2) matrix transformation
m13(W2) direct measurement
m13(W3) direct measurement
m13(W3) matrix transformation
m13(W4) direct measurement
m13(W4) matrix transformation

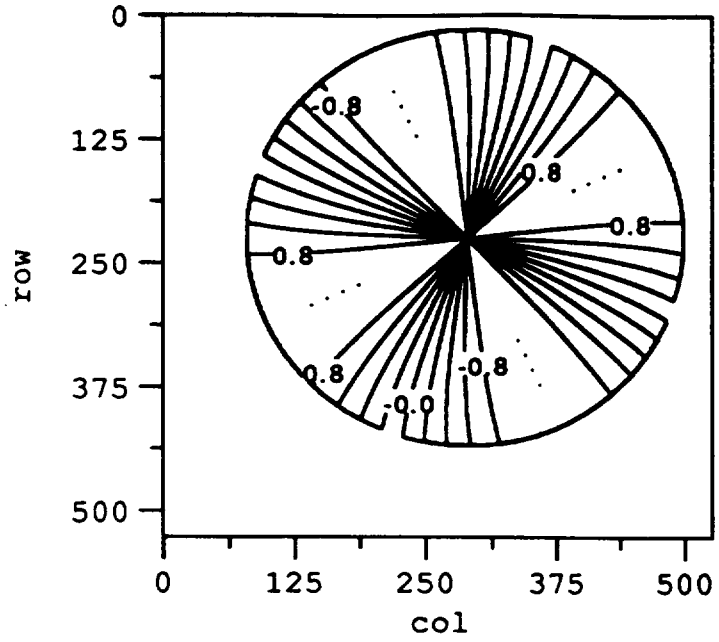
0
125
250
375
500
row
0
125
250
375
500
col
-0.8
0.8
0.8
0.8
0.8
-0.8
-0.0

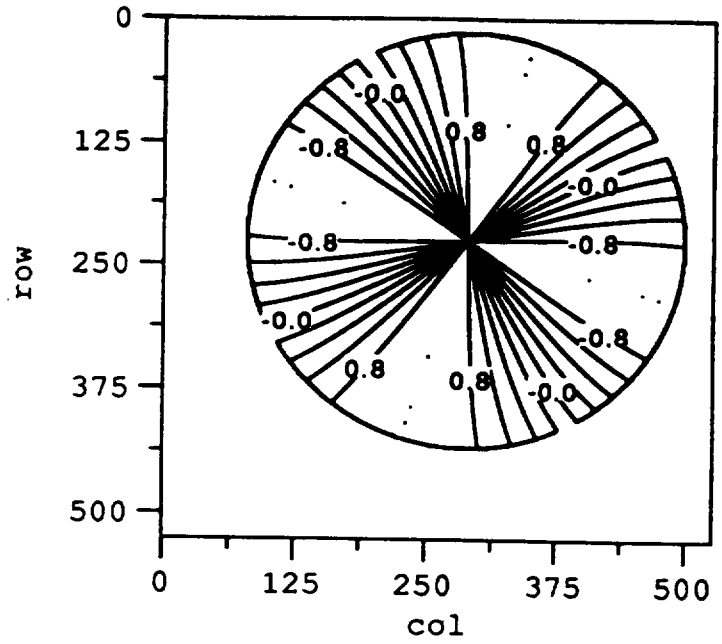
0
125
250
375
500
row
0
125
250
375
500
col
-0.0
0.8
0.8
-0.0
-0.8
-0.8
-0.8
-0.8
-0.0
-0.8
0.8
0.8
-0.0